Structure and Dynamics of Condensed DNA Probed by 1,1′-(4,4,8,8-Tetramethyl-4,8-diazaundecamethylene)bis[4-[[3-methylbenz-1,3-oxazol-2-yl]methylidine]-1,4-dihydroquinolinium] Tetraiodide Fluorescence

G. Krishnamoorthy,*,‡ Guy Duportail, and Yves Mély

Laboratoire de Pharmacologie et Physicochimie des interactions cellulaires et moléculaires, UMR 7034 du CNRS, Faculté de Pharmacie, Université Louis Pasteur de Strasbourg, 74 Route du Rhin, 67401 Illkirch, France

Received June 27, 2002

ABSTRACT: Information on the structure and dynamics of condensed forms of DNA is important in understanding both natural situations such as DNA packaging and artificial systems such as gene delivery complexes. We have established the fluorescence of bisintercalator 1,1′-(4,4,8,8-tetramethyl-4,8-diazaundecamethylene)bis[4-[[3-methylbenz-1,3-oxazol-2-yl]methylidine]-1,4-dihydroquinolinium] tetraiodide (YOYO-1) as a novel probe for DNA condensation. When the level of DNA-bound YOYO-1 is sufficiently large, condensation by either polyethylenimine (PEI) or the cationic detergent cetyltrimethylammonium bromide (CTAB) leads to electronic interaction among YOYO-1 molecules bound on the same DNA molecule. This interaction results in an excitonic blue shift of the absorption spectra of YOYO-1 and dramatic decrease in the fluorescence quantum yield. These observations constitute a signature of the condensation of DNA. We further examined the comparative properties of DNA condensed by PEI, CTAB, or $Co(NH_3)_6^{3+}$ through the steady-state and dynamic fluorescence of YOYO-1. Condensation by either PEI or CTAB was associated with a blue shift in the absorption spectra of YOYO-1, although the magnitude of the shift was larger in the case of PEI when compared to that of CTAB. In contrast, condensation by $Co(NH_3)_6^{3+}$ was not associated with a measurable shift in the absorption spectra. These results were interpreted as signifying the varying level of compactness of the DNA condensates. Quenching of fluorescence by acrylamide showed that condensation by all three agents led to an increase in the level of solvent exposure of the base pairs. Observation of the decay of fluorescence intensity and anisotropy of DNA-bound YOYO-1 showed that while condensation by either PEI or CTAB froze the segmental mobility of the helix, condensation by $Co(NH_3)_6^{3+}$ enhanced the flexibility of DNA. The relevance of our findings to functions such as efficiency of gene delivery is discussed.

Condensation of DNA is a ubiquitous phenomenon encountered in a variety of both natural and artificial situations. Chromatinized DNA in the nucleus of mammalian cells (*1*) and DNA packed into phage heads (*2*) exemplify the phenomenon of natural condensation. Gene delivery systems in which DNA is condensed by polycations (*3*, *4*) and cationic lipids (*5*, *6*) and detergents (*7*) and used to transfect cells both in vitro and in vivo (*8*−*11*) represent the major part of artificial condensation. While the phenomenon of DNA condensation (for a review see ref *12*) has been extensively studied by a variety of imaging (*13*−*17*), single-molecule (*7*, *18*), hydrodynamic (*19*), thermodynamic (*20*), and transfection (*21*) techniques, there is a relative lack of understanding of the driving force for the condensation process (*22*).

Atomic force microscopy (*13*−*16*) and some electron microscopy observations (*17*) have revealed that the condensed form of DNA is characterized by toroidal and rodlike structures of dimensions in the range of 50−100 nm. Recent studies have also captured the images of the various types of intermediates formed during the condensation process (*16*). Although there are some structural studies using X-ray scattering (*23*, *24*) and X-ray diffraction (*1*) on condensed forms of DNA, the atomic level high-resolution structures are lacking. For example, even the question of whether the DNA is wrapped around the condensing agent or vice versa is debatable, although it has been shown that condensation leads to protection from nucleases (*25*). Similarly the information on the base pair and backbone dynamics of condensed DNA is relatively scarce. It has been recognized that condensation of extended DNA polymer into compact particles is essential for entry into cells mainly by the endocytic pathway (*26*). However, the pathway of trafficking of these condensed particles in the cells and the mechanism of transcription of the trafficked DNA are largely unknown. Can transcription occur in the condensed form or only after the dissociation of the condensing agent? Why are some of the condensing agents more efficient than other agents? Answers to such questions require information on the structure and dynamics of condensed DNA apart from the

* To whom correspondence should be addressed at the Tata Institute of Fundamental Research. E-mail: gk@tifr.res.in. Fax: +91-22-215 2110. Phone: +91-22-215 2181.

‡ On leave from the Department of Chemical Sciences, Tata Institute of Fundamental Research, Homi Bhabha Rd., Mumbai 400 005, India.

10.1021/bi020440y CCC: $22.00
Published on Web 11/26/2002

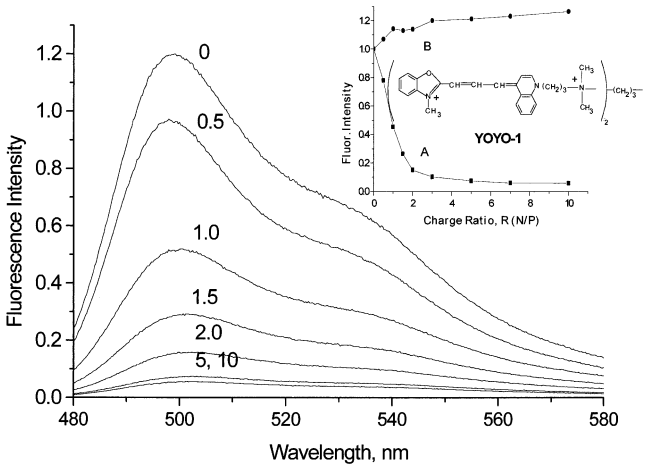

FIGURE 1: Fluorescence emission spectra of the DNA−YOYO-1 complex in the presence of PEI. The charge ratio, *R*, is given for each spectrum. The concentrations of DNA (phosphate) and YOYO-1 were 10 and 0.2 μM, respectively (*D*:*P* = 1:50). The medium was 15 mM HEPES, 0.2 mM EDTA at pH 7.4. The inset shows the plot of integrated fluorescence intensity as a function of *R*. Curve A corresponds to a *D*:*P* ratio of 1:50, and curve B corresponds to a *D*:*P* ratio of 1:2000. The excitation was at 470 nm.

knowledge of the interaction of condensed DNA with as yet unidentified cellular constituents. Knowledge derived from such information could also be used to model the mechanism of transcription of nuclear DNA apart from understanding the overall mechanism of gene delivery. In this work we have established that the bisintercalator YOYO-1[1] (Figure 1, inset) is a useful probe for monitoring DNA condensation. Subsequently we used steady-state and time-resolved fluorescence intensity and anisotropy of YOYO-1 in visualizing some aspects of the structure and dynamics of DNA condensed by a variety of condensing agents. Our study brings out comparative information on hindered rotational dynamics of base pairs and the restrained tortional dynamics of the backbone of condensed DNA.

MATERIALS AND METHODS

Materials. pCMV-luc plasmid (5.2 kbp) was propagated and purified as described (*40*). Branched chain PEI (25 kDa) was a gift from Prof. J.-P. Behr, Illkirch, France. YOYO-1 (491/509) was obtained from Molecular Probes Inc. CTAB, acrylamide, and $Co(NH_3)_6Cl_3$ were from Sigma Chemical Co.

Samples. Plasmid DNA−YOYO-1 complexes were made by mixing equal volumes of solutions of DNA and YOYO-1 in 20 mM HEPES, pH 7.4. The mixed solution was incubated at room temperature for at least 5 h before use. This procedure ensured uniform distribution of YOYO-1, which binds very tightly to DNA. Complexes of plasmid DNA−YOYO-1 with PEI were formed by adding PEI to a solution of DNA followed by vortexing for about 1 min and incubation at room temperature for about 30 min. The ± charge ratio *R* refers to the ratio of the primary nitrogen of PEI (or the concentration of CTAB) to the phosphate of DNA.

[1] Abbreviations: CTAB, cetyltrimethylammonium bromide; DMSO, dimethyl sulfoxide; FRET, fluorescence resonance energy transfer; PEI, polyethylenimine; YOYO-1, 1,1′-(4,4,8,8-tetramethyl-4,8-diazaundecamethylene)bis[4-[[3-methylbenz-1,3-oxazol-2-yl]methylidine]-1,4-dihydroquinolinium] tetraiodide.

Spectroscopic Measurements. Absorption spectra were recorded on a Cary 400 spectrophotometer. A SLM 48000 spectrofluorimeter was used for steady-state fluorescence measurements. Other experimental conditions are given in the figure captions.

Quenching of fluorescence intensity, *I*, by acrylamide was analyzed by the equation

$$I_0/I = 1 + K_{SV}[Q] \quad (1)$$

where I_0 is the intensity in the absence of the quencher, Q, and K_{SV} is the Stern−Volmer quenching constant. Nonlinear quenching curves (I_0/I vs [Q]) were analyzed by the two-population model (*41*, *49*):

$$I/I_0 = \{a/(1 + K_{SV1}[Q]) + b/(1 + K_{SV2}[Q])\} \quad (2)$$

where *a* and *b* are the fractional contributions to the total fluorescence intensity of the two populations characterized by the quenching constants K_{SV1} and K_{SV2}, respectively.

Time-resolved fluorescence intensity and anisotropy measurements on DNA−YOYO-1 complexes and their condensed forms were performed by using the frequency-doubled output of a Ti−sapphire laser (Spectra Physics). The excitation wavelength was 480 nm, and the emission was collected at 515 nm by using a single-photon-counting microchannel plate photomultiplier (Hamamatsu R3809U). Other details are given elsewhere (*28*). The resolution of the time-correlated single-photon-counting setup was 25.5 ps, and the width of the instrument response function was ~40 ps.

Fluorescence intensity decays obtained at the magic angle were deconvoluted with the instrument response function and analyzed as a sum of exponentials:

$$I(t) = \sum \alpha_i \exp(-t/\tau_i) \quad (3)$$

where $I(t)$ is the fluorescence intensity collected at the magic angle at time *t* and α_i is the amplitude of the *i*th lifetime, τ_i, such that $\sum \alpha_i = 1$.

Time-resolved fluorescence anisotropy decays were analyzed by the following equations:

$$I_{||}(t) = I(t)[1 + 2r(t)]/3$$

$$I_{\perp}(t) = I(t)[1 - r(t)]/3$$

$$r(t) = [I_{||}(t) - I_{\perp}(t)]/[I_{||}(t) + 2I_{\perp}(t)] = r_0 \sum \beta_i \exp(-t/\varphi_i) \quad (4)$$

where r_0 is the initial anisotropy and β_i is the amplitude of the *i*th rotational correlation time, φ_i, such that $\sum \beta_i = 1$. $I_{||}$ and $I_{\perp}$ are the intensities collected at emission polarizations parallel and perpendicular, respectively, to the polarization axis of the excitation beam. While the kinetics of anisotropy decay was analyzed, the values of α_i and τ_i (obtained from the analysis of $I(t)$) were kept fixed to reduce the number of floating parameters. This procedure results in better estimates of anisotropy decay parameters.

RESULTS

YOYO-1 as a Novel Probe for DNA Condensation. Figure 1 shows the fluorescence emission spectra of YOYO-1 in

Table 1: Parameters Associated with the Decay of Fluorescence Intensity

sample[a]	*D*:*P*	fluorescence lifetimes[b] (amplitudes), ns			
		τ_1 (α_1)	τ_2 (α_2)	τ_3 (α_3)	τ_{mean}[c]
(1) YOYO-1 in buffer		0.44 (0.03)	0.060 (0.97)		0.070
(2) DNA−YOYO-1, uncondensed form	1:50	4.97 (0.50)	1.97 (0.50)		3.45
(3) DNA−YOYO-1−PEI ($R = 3$)	1:50	4.17 (0.04)[d]	1.60 (0.09)[d]	0.33 (0.08)[d]	1.61
(4) DNA−YOYO-1, uncondensed form	1:2000	5.40 (0.39)	2.23 (0.61)		3.43
(5) DNA−YOYO-1−PEI ($R = 1$)	1:2000	5.40 (0.52)	2.27 (0.48)		3.93
(6) DNA−YOYO-1−PEI ($R = 5$)	1:2000	5.10 (0.70)	2.10 (0.30)		4.18
(7) DNA−YOYO-1−PEI ($R = 10$)	1:2000	5.20 (0.72)	2.02 (0.28)		4.36
(8) DNA−YOYO-1−CTAB ($R = 1$)	1:2000	5.1 (0.56)	2.16 (0.44)		3.83
(9) DNA−YOYO-1−CTAB ($R = 5$)	1:2000	5.2 (0.73)	2.15 (0.27)		4.39
(10) DNA−YOYO-1−CTAB ($R = 10$)	1:2000	5.4 (0.75)	2.22 (0.25)		4.65
(11) DNA−YOYO-1−$Co(NH_3)_6^{3+}$, $[Co^{3+}] = 5\ \mu M$	1:2000	4.1 (0.09)	1.25 (0.61)	0.35 (0.30)	1.22
(12) DNA−YOYO-1−$Co(NH_3)_6^{3+}$, $[Co^{3+}] = 15\ \mu M$	1:2000	3.1 (0.06)	0.98 (0.61)	0.19 (0.33)	0.85
(13) DNA−YOYO-1−$Co(NH_3)_6^{3+}$, $[Co^{3+}] = 40\ \mu M$	1:2000	3.2 (0.03)	0.95 (0.09)	0.11 (0.89)	0.29

[a] The concentration of DNA was 10 μM phosphate and that of YOYO-1 was 5 nM for all the samples. The medium was 15 mM Hepes, 0.2 mM EDTA at pH 7.4. [b] The uncertainties in the parameters are about 5% for τ_1 and τ_2 and about 10% for τ_3. These estimations are based on several observations on the same sample and also analyses on repeat samples. The value of χ^2 was between 1.1 and 1.3 for all the samples. [c] $\tau_{mean} = \sum\alpha_i\tau_i$. [d] The amplitudes, α_{ic}, were recalculated from the experimental amplitudes, α_i, according to $\alpha_{ic} = \alpha_i(1 - \alpha_0)$ to take into account the relative amplitude of the dark species, α_0. This latter parameter is calculated by $\alpha_0 = 1 - \langle\tau\rangle_{DNA}/\langle\tau\rangle_{DNA-PEI}R'$, where $\langle\tau\rangle_{DNA}$ is the mean lifetime of YOYO-1 in the DNA−YOYO-1 complex in the absence of PEI, $\langle\tau\rangle_{DNA-PEI}$ is the measured mean lifetime of YOYO-1 in the corresponding complex with PEI, and R' is the ratio between the steady-state fluorescence intensity of the complex in the absence of PEI and that in the presence of PEI.

the presence of DNA and varying concentrations of PEI. Increasing concentration of PEI led to a dramatic decrease in the fluorescence quantum yield of DNA-bound YOYO-1. In these experiments, the ratio of the concentrations of YOYO-1 and nucleotide (*D*:*P*) was 1:50. The fluorescence intensity of YOYO-1 in the absence of DNA was several orders of magnitude lower when compared to that of the YOYO-1−DNA complex (data not shown), similar to observations by other workers (*27*, *28*). In contrast to the behavior seen at a *D*:*P* ratio of 1:50, the fluorescence intensity did not show any decrease when the ratio *D*:*P* was reduced to 1:2000 (Figure 1, inset). This suggested that the decrease in fluorescence intensity observed at *D*:*P* = 1:50 cannot arise from any change in the environment of individual intercalated YOYO-1 molecules when DNA condensation occurs.

The observation of a decrease in fluorescence intensity at high levels of bound YOYO-1 (*D*:*P* = 1:50 or lower) suggests interaction among DNA-bound YOYO-1 molecules. To check such a hypothesis, the fluorescence lifetime of DNA−YOYO-1 was measured at various concentrations of PEI. The dominant lifetime of aqueous YOYO-1 was about 60 ps (Table 1), consistent with its very low quantum yield. Intercalated YOYO-1 (at *D*:*P* = 1:50) showed two lifetimes. Addition of PEI caused a decrease in the values of the two lifetime components and the appearance of a short one (0.33 ns). However, the very short lifetime value (~60 ps) of the aqueous YOYO-1 was not observed, indicating the absence of free YOYO-1 when the condensation occurred. In contrast to the condensation-induced decrease in the lifetime values at *D*:*P* = 1:50, the lifetime values did not show appreciable changes when the YOYO-1 was sparse in the plasmid DNA (*D*:*P* = 1:2000) as shown in Table 1. These results when seen in conjunction with steady-state fluorescence data (Figure 1) suggest the presence of interaction among YOYO-1 molecules bound within a plasmid condensed by the binding of PEI. This interaction results in a decrease in the quantum yield of YOYO-1.

Interaction among YOYO-1 molecules proposed above was confirmed from their absorption spectra. Figure 2A shows that the absorption spectrum of DNA-bound YOYO-1 (at a *D*:*P* ratio of 1:50) undergoes dramatic changes following PEI-induced condensation of DNA. Such changes were not observed when the level of YOYO-1 was reduced (*D*:*P* > 1:200, data not shown). Various types of intermolecular interactions leading to electronic delocalization have been observed (*29*, *30*, *31* and references therein) in organic dye molecules. J-type and H-type dimers and aggregates are known to have specific signatures in their absorption spectra (*32*). The observed blue shift of the absorption peak (Figure 2A) indicates an H-type geometry as predicted by exciton theory (*32*) of molecular interactions. A similar blue shift of the absorption peak has been observed in many other intermolecular interactions (*29*, *30*).

One of the signatures of close proximity of fluorescent molecules is the donor−donor energy migration leading to fluorescence depolarization (*33*). Figure 3 shows the fluorescence anisotropy decay kinetics of YOYO-1 in PEI-condensed DNA at *D*:*P* values of 1:50 and 1:2000. The striking observation was the significant reduction in the value of zero time anisotropy, r_0, from ~0.2 to ~0.1 when the *D*:*P* ratio was increased from 1:2000 to 1:50 (YOYO-1 concentration increase). Such observations have been made in several other systems and modeled extensively (*33*−*35*). Taken together all these observations point out that the significant decrease in fluorescence intensity of YOYO-1 (at *D*:*P* > 1:50) is due to interaction among YOYO-1 molecules in the condensed DNA and that this signal could be used as an identification and measure of DNA condensation.

DNA Condensation by PEI, CTAB, and Co$(NH_3)_6^{3+}$. The main aim of the current work is to delineate the structure and dynamics of condensed DNA. In this regard it would

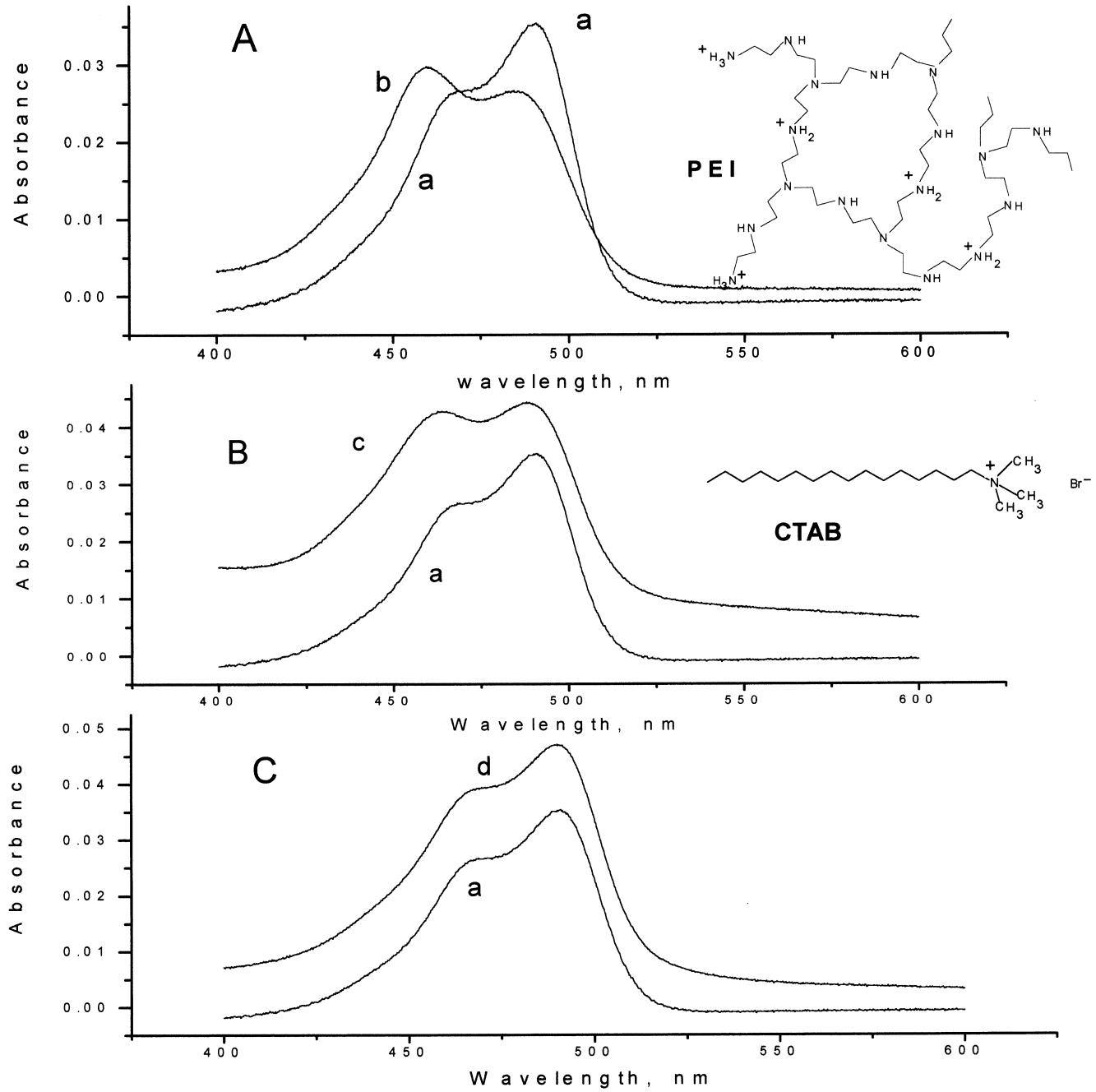

FIGURE 2: Condensation-induced excitonic blue shift in the absorption spectra of DNA-bound YOYO-1. Curves a correspond to uncondensed DNA (10 μM phosphate, *D*:*P* = 1:50). Curves b−d correspond to DNA condensed by PEI (*R* = 6), CTAB (*R* = 6) and $Co(NH_3)_6^{3+}$ (180 μM), respectively. The upward shift in the spectra of condensed DNA is due to light scattering.

be of interest to compare the dynamic aspects when the condensation is caused by a variety of agents. We chose the cross-linked cationic polymer PEI, cationic detergent CTAB, and classical multivalent cation $Co(NH_3)_6^{3+}$ as typical condensing agents for our comparative study. Figure 4 shows the titration of the fluorescence intensity of DNA-bound YOYO-1 by these condensing agents. It can be seen that the condensation signal (i.e., the extent of decrease in fluorescence intensity at a *D*:*P* ratio of 1:50) was stronger with PEI when compared to CTAB. This observation indicates that PEI is more efficient in condensing the DNA when compared to CTAB. The condensation signal was absent when the level of YOYO-1 was reduced (*D*:*P* ratio of 1:2000) as expected. In contrast to the behavior of PEI and CTAB, condensation by the multivalent cation $Co(NH_3)_6^{3+}$ resulted in a dramatic decrease in the fluorescence intensity at all the *D*:*P* ratios (Figure 4e,f). This suggests that the mechanism of quenching of the fluorescence of YOYO-1 during condensation by $Co(NH_3)_6^{3+}$ is unlikely to be due to excitonic interaction among YOYO-1 molecules. This quenching of fluorescence could have been caused by one or more of the following factors: (i) An increased level of solvent exposure of bound YOYO-1 caused by the binding of $Co(NH_3)_6^{3+}$. (ii) Fluorescence resonance energy transfer between YOYO-1 and $Co(NH_3)_6^{3+}$. The weak absorption band of $Co(NH_3)_6^{3+}$ overlaps the emission band of YOYO-1, leading to a Forster critical distance, R_0, of 16 Å. Hence, any decrease in the fluorescence intensity of YOYO-1 by

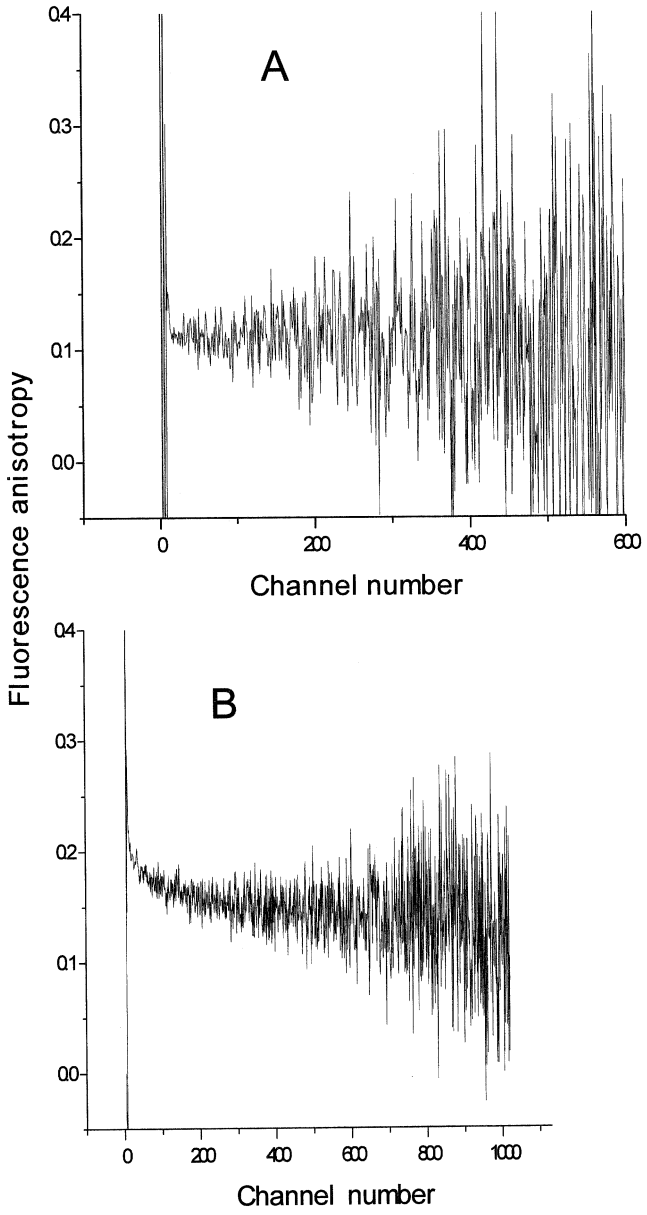

FIGURE 3: Decay of the fluorescence anisotropy of DNA-bound YOYO-1 in PEI-induced DNA condensate at D:P = 1:50 (A) and 1:2000 (B). Note the apparent decrease in initial anisotropy, r_0, from ~0.2 to ~0.1 when the D:P ratio was increased from 1:2000 to 1:50 (increase in the level of YOYO-1). The time resolution was 25.5 ps per channel.

this mechanism would demand the distance between YOYO-1 and $Co(NH_3)_6^{3+}$ be ~16 Å. (iii) The presence of cobalt could result in fluorescence quenching due to heavy-metal-induced intersystem crossing. In fact, intersystem crossing is favored by spin−orbit coupling whose efficiency has a Z^4 dependence (Z is the atomic number).

Figure 2 shows the absorption spectra of DNA-bound YOYO-1 in the presence of the various condensing agents used in this work. The ratio D:P was 1:50 in these experiments. The extent of condensation-induced blue shift was significantly less with CTAB when compared to PEI. In the case of $Co(NH_3)_6^{3+}$ there was no observable change in the absorption spectrum, indicating the absence of discernible interaction among DNA-bound YOYO-1 molecules.

To gain more information on the comparative structures of DNA condensed by the various agents, the accessibility

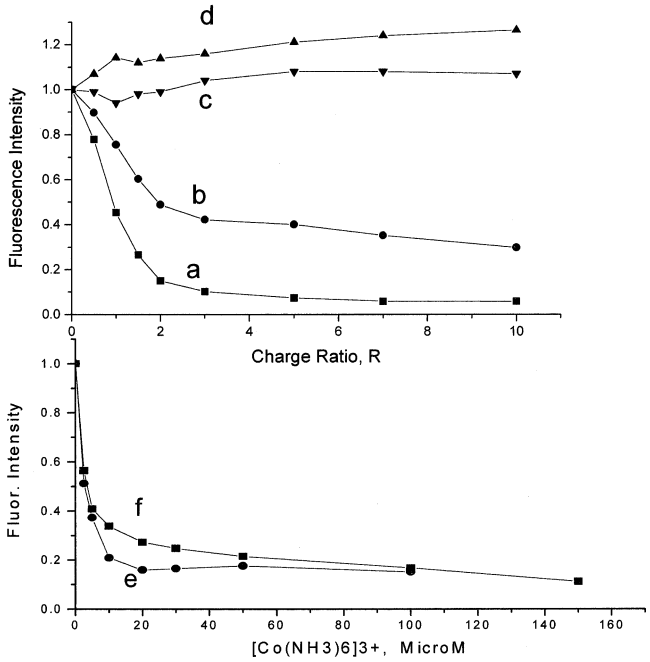

FIGURE 4: Effect on the integrated fluorescence intensity of DNA-bound YOYO-1 on condensation by PEI (a, d), CTAB (b, c), and Co^{3+} (e, f). Curves a, b, and f correspond to a D:P ratio of 1:50 and curves c−e correspond to a D:P ratio of 1:2000. R is the charge ratio in the cases of PEI and CTAB. The concentration of DNA phosphate was 10 μM in the cases of curves e and f.

of bound YOYO-1 to the fluorescence quencher acrylamide was monitored. In these experiments the ratio D:P was 1:2000, and hence, condensation-induced interaction among YOYO-1 molecules will be negligible. Stern−Volmer plots in Figure 5 show that intercalated YOYO-1 is not accessible to acrylamide in uncondensed DNA. Condensation of DNA by all three agents led to an increase in the value of the quenching constant K_{SV} (see the Figure 5 caption), which could be interpreted as increased exposure of the intercalated YOYO-1 (see the Discussion). Two other points are worthy of comment: (i) In the case of CTAB the quenching of fluorescence was more efficient at an R value of unity when compared to $R = 5$. (ii) Quenching in the presence of either $Co(NH_3)_6^{3+}$ or CTAB ($R = 1$) was nonlinear, indicating the presence of more than one type of population (*41*) of bound YOYO-1 in these samples (see the Figure 5 caption).

Dynamic fluorescence parameters such as fluorescence lifetime and fluorescence depolarization time give deep insights into the environment and dynamics of macromolecular systems (*36*). We measured the fluorescence intensity decay of DNA-bound YOYO-1 at a D:P ratio of 1:2000. As mentioned earlier at this ratio YOYO-1 reports mainly the changes in its environment uncomplicated by interactions among YOYO-1 molecules. Table 1 shows typical parameters obtained from the analysis of fluorescence intensity decay kinetics. It was found that the decay kinetics required a sum of at least two exponentials for acceptable fits. It is likely that the two lifetime values of 2.2 ns (61%) and 5.4 ns (39%) represent two modes of binding of YOYO-1. Condensation of DNA by either PEI or CTAB led to a slight increase in the level of population of the longer lifetime component, resulting in an increase in the mean lifetime and hence the fluorescence quantum yield. In contrast, condensation by $Co(NH_3)_6^{3+}$ resulted in significant reduction in the

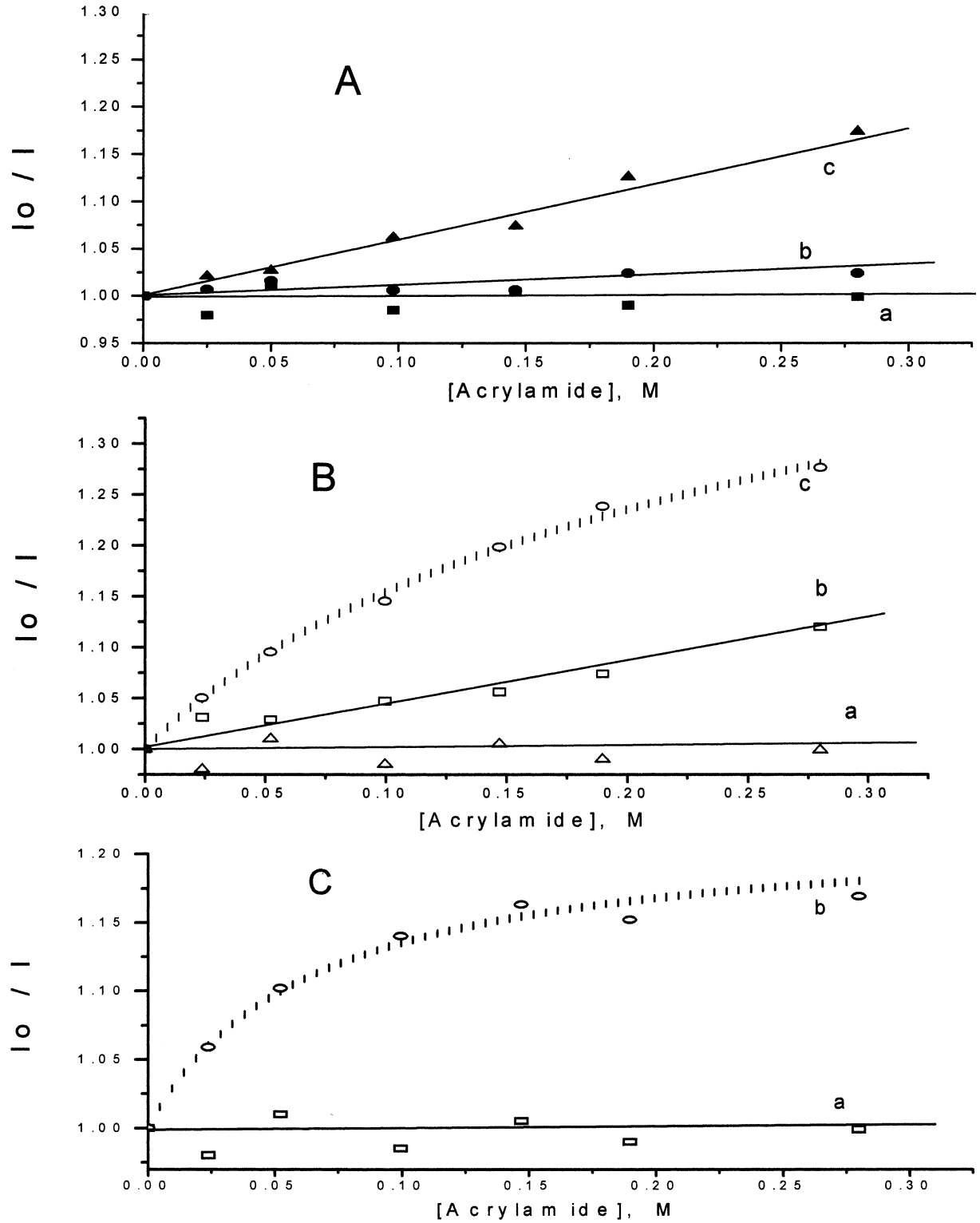

FIGURE 5: Stern−Volmer plots for the quenching of DNA-bound YOYO-1 by acrylamide. I_0 and I are the fluorescence intensities in the absence and in the presence of acrylamide, respectively. In all the panels, curve a corresponds to uncondensed DNA (D:P = 1:2000). (A) Curves b and c correspond to the presence of PEI at R = 1 and 5, respectively. The values of K_{SV} calculated from the slopes are 0.1 and 0.6 M^{-1} for curves b and c, respectively. (B) Curves c and b correspond to the presence of CTAB at R = 1 and 5, respectively. The values of K_{SV} are 0.41 M^{-1} for curve b (R = 6) and 8.4 M^{-1} (27%) and 0.15 M^{-1} (73%) for curve c (R = 1). The nonlinear curve c was fitted with eq 2 given in the text. (C) Curve b corresponds to 40 μM $Co(NH_3)_6^{3+}$. The fitting of this nonlinear curve (eq 2) gave the values of K_{SV} as 9.1 M^{-1} (18%) and $<10^{-2}$ M^{-1} (82%).

mean lifetime, similar to the observations with fluorescence intensity (Figure 1). Further, the complexity of the fluorescence decay kinetics increased, and a minimum of three exponentials were required for satisfactory fits (Table 1). This suggests that significant changes occur in the environment and dynamics of bound YOYO-1 succeeding $Co(NH_3)_6^{3+}$-induced condensation.

The fluorescence depolarization kinetics of DNA-bound YOYO-1 was measured at a D:P ratio of 1:2000. Typical kinetic traces of fluorescence anisotropy decay are shown

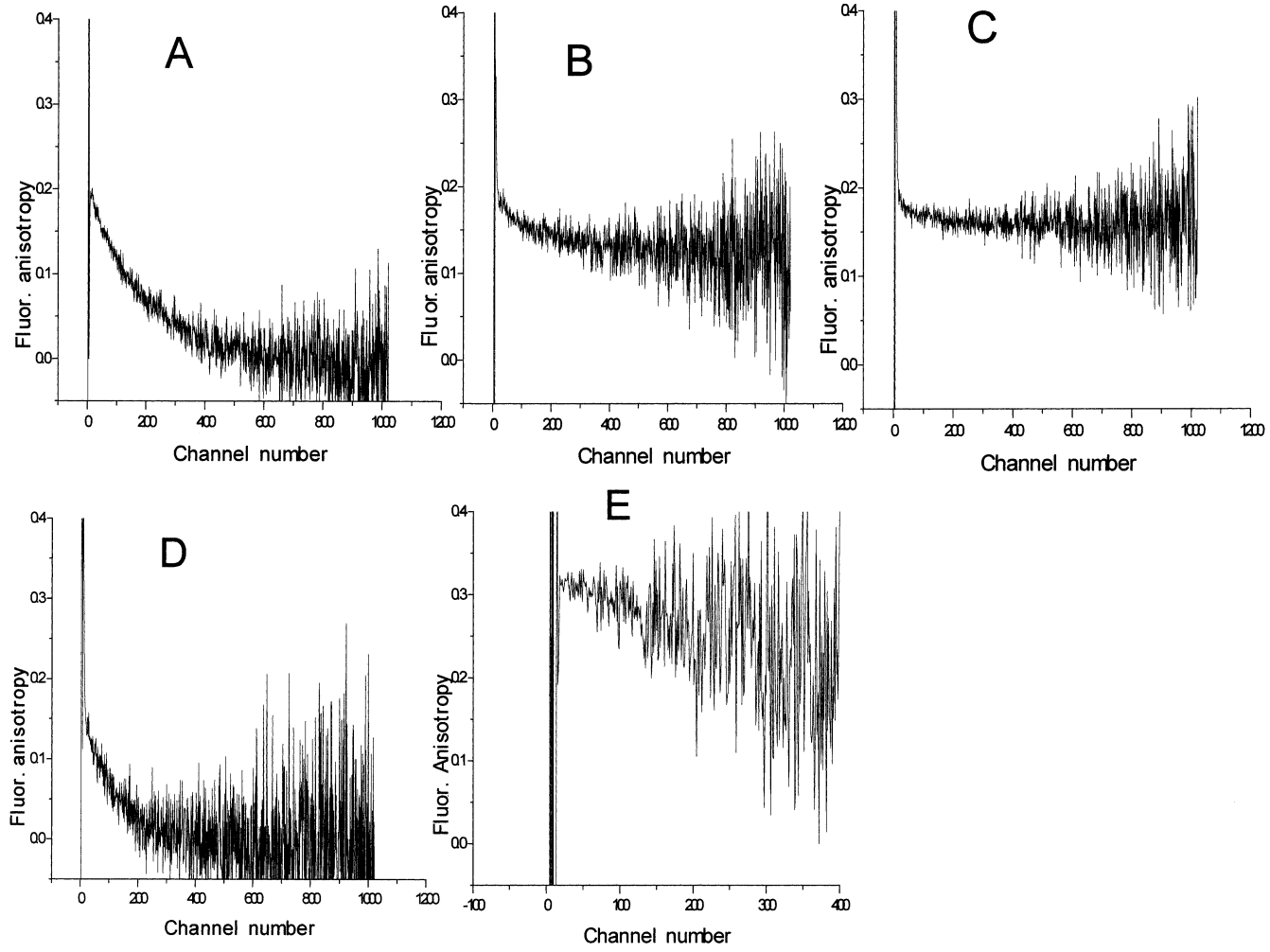

FIGURE 6: Typical traces of the decay of the fluorescence anisotropy of DNA-bound YOYO-1: (A) uncondensed form of DNA; (B) DNA condensed by PEI ($R = 6$); (C) DNA condensed by CTAB ($R = 6$); (D) DNA condensed by Co^{3+} (40 μM); (E) YOYO-1 in 25% DMSO−75% glycerol. The time resolution was 25.5 ps per channel. Parameters obtained from the analysis of these decay curves are given in Table 2.

Table 2: Parameters Associated with the Decay of Fluorescence Anisotropy

sample[a]	R	rotational correlation times[b] (amplitudes), ns			Initial Anisotropy
		φ_1 (β_1)	φ_2 (β_2)	φ_3[c] (β_3)	r_0
(1) DNA−YOYO-1, uncondensed form	0	0.11 (0.41)	4.2 (0.59)		0.31
(2) DNA−YOYO-1−PEI	1	0.12 (0.36)	1.1 (0.20)	>50 (0.44)	0.30
(3) DNA−YOYO-1−PEI	2	0.11 (0.36)	2.1 (0.17)	>50 (0.47)	0.30
(4) DNA−YOYO-1−PEI	5	0.08 (0.37)	1.4 (0.13)	>50 (0.50)	0.31
(5) DNA−YOYO-1−PEI	10	0.06 (0.35)	2.1 (0.16)	>50 (0.49)	0.27
(6) DNA−YOYO-1−CTAB	1	0.10 (0.45)	1.3 (0.10)	>50 (0.45)	0.31
(7) DNA−YOYO-1−CTAB	2	0.08 (0.43)	1.4 (0.12)	>50 (0.45)	0.31
(8) DNA−YOYO-1−CTAB	5	0.07 (0.39)	2.1 (0.10)	>50 (0.51)	0.30
(9) DNA−YOYO-1−CTAB	10	0.11 (0.41)	3.7 (0.09)	>50 (0.50)	0.30
(10) DNA−YOYO-1−$Co(NH_3)_6^{3+}$, $[Co^{3+}] = 40$ μM		0.13 (0.47)	2.9 (0.53)		0.31

[a] All the samples had 10 μM DNA (phosphate concentration) and 5 nM YOYO-1 in 15 mM HEPES, 0.2 mM EDTA at pH 7.4. [b] The levels of uncertainties in the recovered parameters are ~50% in the value of φ_1, ~20% in the value of φ_2, and ~10% in the values of β_i. [c] The value of φ_3 was fixed at >50 ns.

in Figure 6. The decay kinetics in uncondensed plasmid could be satisfactorily fitted to a sum of two exponential functions with time constants $\varphi_1 \approx 0.1$ ns and $\varphi_2 \approx 4$ ns (Table 2). The requirement of fitting to a sum of two exponentials rather than to a single exponential arises from the need to keep the value of the initial anisotropy, r_0, at ~0.31, the value obtained for YOYO-1 in a viscous solvent (25% DMSO−75% glycerol, Figure 6E), where the rotational dynamics is expected to be highly damped. A single-exponential fit gives r_0 as 0.21, which is unrealistic. φ_1 could represent the internal fast motion of YOYO-1, whereas φ_2 could correspond to the motional dynamics of segments of the double-stranded DNA (see the Discussion). Condensation of DNA by any of the three agents led to dramatic changes in the fluorescence

anisotropy decay kinetics (Figure 6). In the cases of PEI and CTAB the overall rate of decay of anisotropy became dramatically slow. Analysis showed that the decays could be satisfactorily fitted to a sum of three exponentials, $\varphi_1 \approx 0.1$ ns, $\varphi_2 \approx 1-3$ ns, and $\varphi_3 > 50$ ns (Table 2). In these analyses also the value of r_0 was kept constant at 0.31 ± 0.01. The lower limit of 50 ns for φ_3 arises due to the limited time window (10−20 ns) offered by the fluorescence lifetime. Again, φ_1 could correspond to internal fast motion of YOYO-1. The limit of ∼30 ps in the time resolution of our experiments cautions us against the interpretation of changes in the value of φ_1. The ∼4 ns component which could represent the segmental dynamics in uncondensed DNA was absent in the DNA condensed by either PEI or CTAB. However, this is replaced by a low-amplitude intermediate dynamics of 1−3 ns and a substantial extent of very slow (>50 ns) dynamics. This could largely represent freezing of the helical backbone by either PEI or CTAB. However, the dynamics observed in the DNA condensed by $Co(NH_3)_6^{3+}$ was strikingly different as a contrast. In this case, the decay of fluorescence anisotropy could be satisfactorily fitted to a sum of two correlation times, $\varphi_1 \approx 0.1$ ns and $\varphi_2 \approx 2.9$ ns (Figure 6 and Table 2). This enhancement of the rate of depolarization could be due to a $Co(NH_3)_6^{3+}$-induced increase in the flexibility of the double-stranded DNA. The amplitude, β_1, associated with the fast internal motion did not change appreciably in the presence of any of the three agents, indicating that condensation has no significant effect on the fast internal motion of YOYO-1.

DISCUSSION

YOYO-1 as a Probe for DNA Condensation. In this work we have shown that the DNA-intercalating dye YOYO-1, when used at sufficiently high concentrations (*D*:*P* ratio of 1:50), could track the process of DNA condensation effectively. The condensation-induced dramatic reduction in the fluorescence quantum yield of DNA-bound YOYO-1 arises only when the ratio *D*:*P* exceeds ∼1:100. This suggests that interaction among YOYO-1 molecules bound to the same DNA molecule could be the cause of the decrease in fluorescence. The most direct support for this model comes from the absorption spectra of YOYO-1 (Figure 2), which show the excitonic blue shift on condensation of DNA. The distance, *R*, between the interacting chromophore dipoles could be estimated from the spectral shift, $\Delta\nu$, by (*32*, *37*)

$$U = (1/4\pi\epsilon_0)(\mu^2/(n^2R^3))\kappa \qquad (5)$$

where U is the interaction energy ($U = hc\Delta\nu$), ϵ_0 is the permittivity of free space, μ^2 is the square module of the transition dipole, n is the refractive index of the medium, and κ is the orientation factor between the two interacting dipoles. In H-type geometry, $\kappa = 1$ (*29*). The value of R calculated for a spectral shift of ∼11 nm (Figure 2A) is ∼12 Å (*30*). This value indicates the distance of closest approach of YOYO molecules and is valid only if all the molecules of YOYO exist as H-dimers. Since there is a possibility of monomers of YOYO coexisting along with H-dimers (see below), the estimate of R should be considered an upper limit.

H-type dimers seen in many systems (*29*, *30*) show no detectable fluorescence. Hence, we could expect a reduction in the fluorescence intensity with no change either in the individual fluorescence lifetimes or in the mean fluorescence lifetime during the transition from monomer to dimer subject to the condition that both monomers and dimers are present. In contrast to this expectation, we see significant reduction in the fluorescence intensity (Figure 1) as well as in the lifetime values (Table 1) during the condensation process, which brings about an interaction among YOYO molecules. The radiative rate constant, k_{rd}, associated with the transition from the lowest electronic excited state to the ground level of the dimer is given by (*29*)

$$k_{rd} = k_{rm}(1 - (\text{sign } \kappa) \cos \theta_{12}) \qquad (6)$$

where k_{rm} is the radiative rate constant associated with the monomer and θ_{12} is the angle between the transition dipoles in the dimer. sign $\kappa = +1$ when $\kappa > 0$, and sign $\kappa = -1$ when $\kappa < 0$. This expression shows that k_{rd} is zero *only* for a perfect H geometry for which $\kappa = 1$ and $\cos \theta_{12} = 1$. A nonzero value of k_{rd} would arise for any value of θ_{12} other than zero. Thus, the observed reduction in the lifetime values could correspond to such a situation. The ratio between the radiative rate constants is given by

$$k_{rd}/k_{rm} = (\tau_m/\tau_d)/(q_m/q_d) \qquad (7)$$

where τ_m and τ_d are the observed fluorescence lifetimes of the monomer and dimer and the q values are the respective quantum yields. Using the condensation-induced changes in the values of the mean lifetimes (Table 1, lines 2 and 3) and fluorescence intensities (Figure 1), we estimate the ratio of the radiative rate constants as ∼0.4, which gives us an estimate of θ_{12} as ∼48°.

An alternative model for explaining the dynamics of YOYO during the condensation process could be as follows: When there is a sufficiently high level of YOYO bound to DNA (*D*:*P* < 1:50), condensation leads to two populations. One of them is the H-dimer with no detectable level of fluorescence ($k_{rd} = 0$), and the other is the residual level of monomers of YOYO. The observation of lifetime values ($\tau_1 \approx 4.2$ ns and $\tau_2 \approx 1.6$ ns, Table 1, line 3) similar to that of the monomers (in the uncondensed DNA, Table 1, line 2) supports this model. To rationalize the time-resolved data (Table 1, lines 2 and 3) with the observed reduction in the fluorescence intensity (Figure 1), we recalculate the amplitudes of the three lifetime components (Table 1, line 3) by taking into account the presence of the dark population of H-dimers. Such a calculation (shown in Table 1, footnote *d*) shows that 79% of the YOYO molecules are present as H-dimers, which represent the dark population. The observation of a short-lifetime component ($\tau_3 \approx 0.33$ ns) in the condensed DNA could originate from FRET from a fraction of YOYO monomers to the dark H-dimers. Estimates based on the absorption spectra of YOYO in condensed DNA and the fluorescence emission spectra give a value of $R_0 \approx 46$ Å. Hence, we could estimate, from the lifetime value of 0.33 ns, the distance of closest approach between the monomer and the H-dimer to be ∼32 Å. This model (with dark H-dimers and fluorescent monomers) appears more realistic when compared to the previous model wherein we considered a uniform population of H-type dimers having a nonzero fluorescence yield.

One could expect the population of monomers of YOYO in condensed DNA to be quite close to each other. This could

lead to excitation energy migration among the monomers by the mechanism of homo-FRET (*33*−*35*, *38*). Energy migration results in time, *t*, dependent fluorescence anisotropy, $r(t)$

$$r(t) = (1/10)((3 - 3\cos^2\theta_{12})e^{-2\omega t} + 3\cos^2\theta_{12} + 1) \quad (8)$$

according to the model of Tanaka and Mataka (*38*). The energy-transfer rate, ω, is given by

$$\omega = (3/2)\langle\kappa^2\rangle(R_0/R)^6\tau_d^{-1} \quad (9)$$

where $\langle\kappa^2\rangle$ is the orientation factor, R_0 is the Forster radius, R is the distance to the nearest neighbor, and τ_d is the fluorescence lifetime of the YOYO-1 monomer. The apparent condensation-induced decrease in the value of r_0 from ∼0.2 to ∼0.1 (Figure 3) would require the time constant associated with the energy-transfer-induced depolarization rate (eq 8) to be <10 ps, which is the lower limit of our time resolution. Estimates based on the values of R_0 (47 Å) and τ_d and lower limit of the time constant (<10 ps) give the value of R as <25 Å. This is reasonable when we consider the overall dimension of the condensed DNA (∼50−100 nm) and the fact that nearly 250 molecules of YOYO are bound in a single plasmid DNA.

Thus, the overall model for explaining the condensation-induced decrease in the fluorescence intensity would involve clustering of the YOYO molecules in a single molecule of plasmid DNA. This clustering is expected to result in at least two classes of distance between YOYO molecules: one with very short distances, leading to excitonic interaction, and another with longer distances, leading to fluorescence resonance energy transfer. Furthermore, our results and analysis show clearly that YOYO-1 remains bound to DNA even after condensation, unlike other intercalating probes such as ethidium, which gets expelled on condensation.

Structure and Dynamics of Condensed DNA. Although condensation of DNA has been achieved by a large variety of agents and procedures (*3*−*11*), only very few forms of condensed DNA are effective as transfection agents. Condensates which interact with the extracellular side of the plasma membrane are unable to achieve transfection since the interaction leads to release of DNA, which gets trapped on the cell surface (*28*). On the other hand, the reduced efficiency of some compact condensates with dimerizable detergents is attributed to the inability of the complex to release the DNA (*39*). Hence, knowledge of the structure and dynamics of condensed DNA would be useful in designing efficient vectors.

PEI has been shown to be one of the very efficient nonviral vectors when compared to other carriers such as CTAB or cationic lipids (*40*). We observed that the level of compactness is higher in the case of PEI when compared to CTAB as seen from both condensation-induced quenching of the fluorescence of YOYO-1 (Figure 4) and the excitonic blue shift in the absorption spectra (Figure 2). The less compact nature of the CTAB−DNA complex could have been the cause for binding to lipid vesicle membranes and subsequent premature release of DNA (*28*). The level of compactness was further assessed through the fluorescence properties of bound YOYO-1. Diffusional quenching of fluorescence by acrylamide (Figure 5) showed that condensation by either CTAB or PEI led to enhanced accessibility of the intercalated YOYO-1. This conclusion is the outcome of the observations that the Stern−Volmer quenching constant, K_{SV} ($=k_Q\tau$), increases on condensation while the fluorescence lifetime is largely invariant (Table 1, *D*:*P* = 1:2000). This indicates an increase in the value of the quenching rate constant, k_Q. Distortion of the secondary structure of DNA and bending of the helix accompany condensation (*12*). Such structural alterations could lead to exposure of the base pairs to the solvent. However, this exposure is likely to be limited only to small molecules and not to nucleases, against which protection is offered by the condensing agents (*25*). In the case of CTAB, the extent of the increase in k_Q was significantly larger in the case of charge ratio $R = 1$ when compared to $R = 5$ (Figure 5). This counterintuitive result could be rationalized on the basis of the model wherein micelle-like clusters having a core of CTAB molecules covered by the DNA are the predominant structures formed at $R = 1$ (*28*). Such curved DNA structures could result in a high level of exposure of base pairs. A further increase in the level of CTAB ($R = 5$) could cover the DNA in an overall manner, leading to a decrease in the level of accessibility. Such a transition from one structural form to another is unlikely in the case of the cross-linked polymer PEI, which is likely to engulf the DNA at all concentrations.

Valuable information on the dynamics of condensed DNA could be gained by time-resolved fluorescence of the intercalated YOYO-1. First, the remarkable increase, by several orders of magnitude, of the quantum yield and fluorescence lifetime of YOYO-1 on binding to DNA has been attributed mainly to the freezing of the internal motion of YOYO-1. Internal-motion-mediated nonradiative decay has been suggested to be the main pathway of deexcitation (*42*). Hence, the insignificant changes in both the quantum yield and lifetime during condensation induced by either PEI or CTAB (under sparse levels of YOYO-1 such as a *D*:*P* ratio of 1:2000) indicate that the internal motion of YOYO-1 and hence that of the base pair do not get enhanced. On the contrary, the small but reproducible increase in both the intensity and mean fluorescence lifetime seen after condensation suggests a further decrease in the level of flexibility. Time-resolved fluorescence anisotropy offers more direct information on the motional dynamics of YOYO-1 and hence the dynamics of base pairs and the helical backbone. It should be mentioned that the major contributor to the body of information on the torsional dynamics of DNA is the studies on fluorescence depolarization of intercalated ethidium bromide (*43*−*45*). (Unfortunately we could not use ethidium bromide in our studies since it gets expelled from condensed DNA (*28*). The much stronger binding bisintercalator YOYO-1 remains bound in condensed DNA and hence was chosen for our studies.) The fluorescence depolarization kinetics of DNA-bound YOYO-1 revealed the presence of a fast (<0.2 ns) internal motion and a slower (∼4 ns) motion which could be ascribed to segmental motion of the double helix (see the Results). The relative amplitude of the fast motion when plugged into the cone angle model of rotational dynamics (*46*) gives us the cone angle associated with the restricted fast motion as 34°. It is likely that this internal motion of YOYO-1 is a reflection of the motional freedom of DNA base pairs (*47*). Condensation by either PEI or CTAB led to freezing of the slower segmental motion but

preservation of the faster internal motion. While freezing of the segmental motion by the condensing agent could be thought of as an expected result, the prevalence of the internal motion, φ_1, is somewhat surprising. The low-amplitude intermediate level motional dynamics ($\varphi_2 \approx 1-3$ ns, Table 2) could correspond to residual level segmental flexibility of the helix in the condensed form. Inspection of the amplitude, β_2, associated with this motion shows that this motion is less prominent in the CTAB−DNA complex when compared to PEI−DNA. This could indicate that the flexibility of the helical backbone is less in the CTAB−DNA complex and the overall compactness is also less when compared to those of the PEI−DNA complex as seen from both the extent of the condensation signal (Figure 4a) and the excitonic blue shift (Figure 2). Such an inference may not look contradictory when we note that the two (PEI−DNA and CTAB−DNA) complexes have significantly different structures and hence could have unrelated properties.

The behavior of DNA condensed by $Co(NH_3)_6^{3+}$ is remarkably different from that condensed by either PEI or CTAB. First, the strong quenching of the fluorescence of YOYO-1 even at very sparse levels (a *D*:*P* ratio of 1:2000, Figure 4e) indicates either that YOYO-1 and most likely the base pairs get exposed to the solvent or that the internal motion of YOYO-1 gets significantly enhanced. Quenching of fluorescence by acrylamide has indicated at least two populations with k_q values of $\sim 10^{10}$ and $< 10^7$ M^{-1} s^{-1} (see the Figure 5 caption). The decrease in the value of the fluorescence lifetime and more importantly in the value of the rotational correlation time (Table 2) ascribed to the segmental motion of the helix indicates that condensation by $Co(NH_3)_6^{3+}$ leads to increased flexibility of the helix. This interpretation is in agreement with the observation that the persistence length of DNA decreases in the presence of Co^{3+} (*48*). Binding of $Co(NH_3)_6^{3+}$ results in bending of the double helix (*48*). Further, the DNA−$Co(NH_3)_6^{3+}$ complex is less compact when compared to the complexes with either PEI or CTAB as seen from the absence of detectable excitonic interaction among bound YOYO-1 molecules in the presence of $Co(NH_3)_6^{3+}$ (Figure 2). Such differences in the properties of DNA condensed by either PEI or CTAB on one hand and by $Co(NH_3)_6^{3+}$ on the other are surprising when one looks at the microscopy images of DNA condensed by either PEI (*13*) or $Co(NH_3)_6^{3+}$ (*14*). In both cases the main feature of the structures is their toroidal nature. One could rationalize these observations by noting that the AFM images are not of atomic resolution and the differences observed by us are a manifestation of subtle differences in the fine structure of the condensates.

ACKNOWLEDGMENT

We thank Mr. David Lleres for the isolation and characterization of the plasmid and Prof. N. Periasamy (TIFR, Mumbai, India) for providing us with the software used in the analysis of time-resolved fluorescence data. G.K. was a fellow from the Ministère de la Recherche. This work was supported by the University Louis Pasteur, CNRS, and the Association Française contre les Myopathies.

REFERENCES

1. Arents, G., and Moudrianakis, E. N. (1993) *Proc. Natl. Acad. Sci. U.S.A. 90*, 10489−10493.
2. Shellman, J. A., and Parthasarathy, N. (1984) *J. Mol. Biol. 175*, 313−329.
3. Behr, J.-P. (1993) *Acc. Chem. Res. 26*, 274−278.
4. Tang, M. X., and Szoka, F. C. (1997) *Gene Ther. 4*, 823−832.
5. Miller, A. D. (1998) *Angew Chem. Int. Ed. 37*, 1768−1785.
6. Tarahovsky, Y. S., Rakhmanova, V. A., Epand, R. M., and MacDonald, R. C. (2002) *Biophys. J. 82*, 264−273.
7. Mel'nikov, S. M., Sergeyev, V. G., Melnikova, Y. S., and Yoshikawa (1997) *J. Chem. Soc., Faraday Trans. 93*, 283−288.
8. Abadalla, B., Hassan, A., Benoist, C., Goula, D., Behr, J.-P., and Demeneix, B. A. (1996) *Hum. Gene Ther. 7*, 1947−1954.
9. Goula, D., Remy, J. S., Erbacher, P., Wasowicz, M., Levi, G., Abadalla, B., and Demeneix, B. A. (1998) *Gene Ther. 5*, 712−717.
10. Goula, D., Benoist, C., Mantero, S., Merlo, G., Levi, G., and Demeneix, B. A. (1998) *Gene Ther. 5*, 1291−1295.
11. Nair, R. R., Rodgers, J. R., and Schwarz, L. A. (2002) *Mol. Ther. 5*, 455−462.
12. Bloomfield, V. A. (1996) *Curr. Opin. Struct. Biol. 6*, 334−341.
13. Dunlap, D. D., Maggi, A., Soria, M. R., and Monaco, L. (1997) *Nucleic Acids Res. 25*, 3095−3101.
14. Arscott, P. G., Ma, C., Wenner, J. R., and Bloomfield, V. A. (1995) *Biopolymers 36*, 345−364.
15. Golan, R., Pietrasanta, L. I., Hsieh, W., and Hansma, H. G. (1999) *Biochemistry 38*, 14069−14076.
16. Martin, A. L., Davies, M. C., Rackstraw, B. J., Roberts, C. J., Stolnik, S., Tendler, S. J. B, and Williams, P. M. (2000) *FEBS Lett. 480*, 106−112.
17. Hud, N. V., and Downing, K. H. (2001) *Proc. Natl. Acad. Sci. U.S.A. 98*, 14925−14930.
18. Kral, T., Langner, M., Benes, M., Baczynska, D., Ugorski, M., and Hof, M. (2002) *Biophys. Chem. 95*, 135−144.
19. He, S., Arscott., and Bloomfield, V. A. (2000) *Biopolymers 53*, 329−341.
20. Matulis, D., Rouzina, I., and Bloomfield, V. A. (2000) *J. Mol. Biol. 296*, 1053−1063.
21. Daught, E., Remy, J.-S., Blessing, T., and Behr, J.-P. (2001) *J. Am. Chem. Soc. 123*, 9227−9234.
22. Bloomfield, V. A. (1997) *Biopolymers 44*, 269−282.
23. Pitard, B., Oudrhiri, N., Vigneron, J. P., Hauchecorne, M., Aguerre, O., Toury, R., Airiau, M., Ramaswamy, R., Scherman, D., Crouzet, J., Lehn, J. M., and Lehn, P. (1999) *Proc. Natl. Acad. Sci. U.S.A. 96*, 2621−2626.
24. Maccioni, E., Vergani, L., Dembo, A., Mascetti, G., and Nicolini, C. (1998) *Mol. Biol. Rep. 25*, 73−86.
25. Moret, I., Peris, J. E., Guillem, V. M., Benet, M., Revert, F., Dasi, F., Crespo, A., and Alino, J. (2001) *J. Controlled Release 76*, 169−181.
26. Remy-Kristensen, A., Clamme, J.-P., Vuilleumier, C., Kuhry, J.-G., and Mely, Y. (2001) *Biochim. Biophys. Acta 1514*, 21−32.
27. Larsson, A., Carisson, C., and Jonsson, M. (1995) *Biopolymers 36*, 153−167.
28. Clamme, J.-P., Bernacchi, S., Vuilleumier, C., Duportail, G., and Mely, Y. (2000) *Biochim. Biophys. Acta 1467*, 347−361.
29. Packard, B. Z., Toptygin, D. D., Komoriya, A., and Brand, L. (1996) *Proc. Natl. Acad. Sci. U.S.A. 93*, 11640−11645.
30. Bernacchi, S., and Mely, Y. (2001) *Nucleic Acids Res. 29*, e62.
31. Wang, M., Silva, G. L., and Armitage, B. A. (2000) *J. Am. Chem. Soc. 122*, 9977−9986.
32. Kasha, M. (1963) *Radiat. Res. 20*, 55−71.
33. Craver, F. W., and Knox, R. S. (1971) *Mol. Phys. 22*, 385−402.
34. Gautier, I., Tramier, M., Durieux, C., Coppey, J., Pansu, R. B., Nicolas, J.-C., Kemnitz, K., and Coppey-Moisan, M. (2001) *Biophys. J. 80*, 3000−3008.
35. Runnels, L. W., and Scarlata, S. F. (1995) *Biophys. J. 69*, 1569−1583.
36. Millar, D. P. (2000) *Methods Enzymol. 323*, 442−459.
37. Scholes, D. S., and Ghiggino, K. P. (1994) *J. Phys. Chem. 98*, 4580−4590.
38. Tanaka, F., and Mataga, N. (1979) *Photochem. Photobiol. 29*, 1091−1097.
39. Blessing, T., Remy, J.-S., and Behr, J.-P. (1998) *Proc. Natl. Acad. Sci. U.S.A. 95*, 1427−1431.
40. Boussif, O., Lezoualc'h, F., Zanata, M. A., Mergny, M. D., Scerman, D., Demeneix, B., and Behr, J.-P. (1995) *Proc. Natl. Acad. Sci. U.S.A. 92*, 7297−7301.
41. Eftink, M. R. (1991) in *Topics in Fluorescence Spectroscopy* (Lakowicz, J. R., Ed.) Vol. 2, pp 53−126, Plenum Press, New York.

42. Carlsson, C., Larsson, A., Jonsson, M., Albinsson, B., and Norden, B. (1994) *J. Phys. Chem. 98*, 10313−10321.
43. Millar, D. P., Robbins, R. J., and Zewail, A. H. (1982) *J. Chem. Phys. 76*, 2080−2094.
44. Schurr, J. M., Fujimoto, B. S., Wu, P., and Song, L. (1992) in *Topics in Fluorescence Spectroscopy* (Lakowicz, J. R., Ed.) Vol. 3, pp 137−229, Plenum Press, New York.
45. Chirico, G., Collini, M., Toth, K., Brun, N., and Langowski, J. (2001), *Eur. Biophys. J. 29*, 597−606.
46. Kinoshita, K. J., Kawato, S., and Ikegami, A. (1977) *Biophys. J. 20*, 289-
47. Georghiou, S., Bradrick, T. D., Philippetis, A., and Beechem, J. M. (1996) *Biophys. J. 70*, 1909−1922.
48. Porschke, D. (1986) *J. Biomol. Struct. Dyn. 4*, 373−389.
49. Swaminathan, R., Periasamy, N., Udgaonkar, J. B., and Krishnamoorthy, G. (1994) *J. Phys. Chem. 98*, 9270−9278.

BI020440Y